Nanometer-scale investigations into oil-rich chalk formations

N. Wang[1] & C. Durkan[1,*]

[1] : The Nanoscience centre, University of Cambridge, 11 JJ Thomson Avenue, Cambridge, CB3 0FF

[*] : Corresponding Author, email: cd229@eng.cam.ac.uk

Core samples from two different depths of a Carbonate oil field have been investigated using optical and electron microscopy, elemental mapping and atomic force microscopy. The sample from the greater depth displays a striking magnetic response, greater compaction and cementation of coccoliths, and an oily film on all surfaces, whereas the sample from higher up shows no magnetic response, no oily film and less well-developed coccoliths. Our results reveal the link between oil formation and the presence of iron compounds.

Introduction

Coccoliths are one of the most important groups of primary products in the ocean: carbonates [1]. They are micrometre-scale disk-like structures comprised of single crystal calcite units that have been grown by unicellular marine algae (coccolithophores) [2], [3], [4]. The algae do so by capturing CO_2, representing a significant component of the carbon cycle. These inorganic structures ultimately sink to the seabed taking residual algae with them, and over time via the build up of these sedimentary deposits which also incorporate sand and other marine organisms, chalk is formed [5], [6]. This deposition is a continuous process, with significant spatial and temporal variations across the planet, depending on the exact nature of the algae in that region, which in turn depend on available nutrients, temperature, atmospheric CO_2 levels and other factors, including the presence of iron, which is known to promote algal growth [7]. As a result, different strata of the resulting chalk formations contain different coccolith populations, and this has been used to track changes in atmospheric CO_2 levels over millennia. As the pressure experienced by any given stratum increases over time due to this continuous deposition from above, the temperature starts to increase, and the by-products of the decomposition of those algae followed by their exposure to the combination of high pressures and temperatures over a long timescale leads to the formation of crude oil. Coccolithophore alkenones serve as the key raw materials for subsurface fossil crude oils. [5]. As oil is formed in the interstitial spaces and on the surfaces of chalk, then in order to understand how to retrieve as much of that oil as possible, it is important to understand the properties of the surfaces and interfaces involved [3]. In this article, we present results from an Atomic Force Microscopy (AFM), Scanning Electron Microscopy (SEM) and Superconducting Quantum Interference Device (SQUID) magnetometry study of the surface morphology and magnetic properties of chalk samples from an oil field in the North Sea. The samples come from two different depths, corresponding to two different time periods of deposition. Both samples possess completely different properties in terms of the number of coccoliths present, their gross morphology, their composition and their magnetic properties, indicative of the variations in conditions mentioned above as well as in the local iron concentration in the ocean at those times.

As well as their intrinsic role in oil and chalk formation, these coccolithophores have exciting potential for advances in nano-fabrication. The genetics, assembly and morphogenesis of the coccoliths (organo-crystalline composites) are under the direct control of the organism and remain virtually unexplored by modern tools.

Previous observations of coccolith structures have been extensive, employing optical, electron and to a limited extent, scanning probe microscopy. Young etc. investigated the crystallographic orientation of the calcite crystal elements of *R. clavigera* spines by Transmission Electron Microscopy (TEM) and Scanning Electron Microscopy (SEM) in conjunction with selected area electron diffraction (SAED) analysis. They also combined this with a nanoscale 3D topographic reconstruction using high-angle annular dark field (HAADF) imaging by Scanning TEM (STEM)[8].

Atomic Force Microscopy (AFM) is the technique of choice for microscopy of samples that have characteristic features with a lateral extent anywhere from around 1 nm to a few tens of microns. However, the vertical (z) range of most AFMs is of order 10 microns. It is this limited z range that is responsible for the small number of reports using this technique as it is extremely challenging to find a meaningful and representative area with small enough variations in surface topography to allow a large lateral area to be selected. On a typical sample, the surface can have variations in height of tens of microns on a lateral scale of a few microns. In this article, we have combined the high lateral resolution of SEM with the high lateral and vertical resolution of AFM, as they complement each other and allow us to have a detailed picture of the overall morphology of the core samples. The addition of EDX provides spatially-resolved elemental mapping, adding a further level of detail to the morphological information provided by SEM and AFM. Finally, the introduction of SQUID measurements complements all of the above, and reveals the fact that the Fe which was observed in one of the samples via EDX leads to the sample having magnetic properties.

Materials and methods

Samples and preparation

Offcut samples from a carbonate field in the North Sea were provided by BP, direct from the drill bore, without having gone through any washing or cleaning procedures. Sample 1 was taken from a depth of 1529 m and sample 2 from a depth of 1922 m. One of the most obvious differences between both samples was that sample 2 had an oily residue on the surface as well as an oily smell, whereas sample 1 did not, and sample 2 was slightly darker in appearance than sample 1. To prepare the samples for AFM experiments, small pieces a few cubic mm in size were removed (by cutting), and fixed to a sample plate using Apiezon wax to (i) minimise drift (ii) ensure the top surface is horizontal. This was necessary as the pieces as cut were generally irregularly shaped. Due to the high sample roughness, in only a few cases was it possible to image large-scale areas up to 50 microns across, and most of the imaged areas were around 10 microns across. In order to obtain information about large-scale features, we took the approach of slicing the samples with a diamond saw, using deionised water as lubricant, resulting in areas with a roughness of a few hundred nm. Although much of the resulting surface was not originally a surface that had been in contact with oil (i.e. was internal to a coccolith or calcite crystal), this opens the possibility to observe structures that would otherwise be missed. It also allowed us to repeatedly return to the same area many different times with different AFM tips, which was rarely the case with the uncut samples. Both samples as well as a sample of crude oil were tested in a SQUID magnetometer to explore differences in magnetic susceptibility. These were then further

explored by EDX (Energy-dispersive X-ray Spectroscopy), which allowed us to obtain elemental maps across the samples.

Instrumentation

All samples were inspected using an Olympus BX51 optical microscope. After AFM imaging, 20 nm of C was sputtered on offcuts of both samples and they were observed using scanning electron microscopy (LEO VP1530). Two different AFMs were used to image the samples: a Park XE-100, and an NT-MDT Solver Pro-M. All images were obtained in tapping-mode under ambient conditions, using Appnano Tapping Mode Sensa Probes (Length=125 microns, resonance frequency = 300 kHz, stiffness= 40 N/m; with reflex coating). Elemental mapping was performed using the EDX module of the same SEM, at an accelerating voltage of 15 kV.

Results and discussion

Optical Microscopy

The typical appearance of the samples as seen using optical microscopy is shown in Figs. 1 and 2 which show sample 1 and sample 2, respectively. The differences between the two samples are clear in terms of their gross morphology and colour. Sample 1 has a white sandy appearance whereas sample 2 has a glossy appearance, indicative of greater compaction, and also contains a large number of orange/brown regions several microns in size.

SEM

Both samples in their original state were imaged by SEM, from which the differences are also apparent. Sample 1 contains a large number of coccoliths, coccospheres and globigernids, many of which are relatively intact, and some of which are shown in Fig. 3. The coccoliths are typically in the size range 2-10 microns across, 0.5 microns thick, and they come in a variety of shapes most of which are elliptical, but with some non-elliptical exceptions. The three gross morphologies murolith, placolith and planolith are all observed. In Figs. 3(a) and (b), placolith-shaped coccoliths are indicated. These are characterised by a well-developed rim comprising interleaved calcite plates arranged around a central hollow region. A planolith structure is shown in Fig. 3(c), again with interleaved plates comprising the rim, but with a closed central area. In a few cases, relatively intact coccospheres were observed, as shown in Fig. 3(d) – on this sample, they all comprise placolith subunits. By contrast, sample 2 has a completely different appearance, as shown in Fig. 4. The most striking differences are that (i) there are a large number of micron-sized crystals, distributed in clusters across the sample and (ii) there is a smooth substance covering much of the surface as shown in Fig. 4(b), whose appearance is similar to that of previously reported SEM analysis of paraffin/waxy components of oil [9]. The gross morphology of the coccoliths is also subtly different in this sample as seen in Fig. 4(c), where further, oriented crystalline growth has occurred on the coccolith platelet surfaces. Similar shaped structures have been reported elsewhere in AFM studies, and have been interpreted as being clay [10]. The crystal dendrites are roughly oriented in a hexagonal arrangement, consistent with clay structures, as well as the hexagonal/rhombohedral structure of calcite, so on the

basis of imaging alone, we cannot determine whether we are seeing overgrowth and early-stage diagenesis or the presence of clay. However, our EDX measurements confirm the presence of Aluminium in this sample, indicating that this is likely to be clay.

EDX

We conducted elemental mapping using EDX on both samples in order to further probe the differences between them.

The SEM/EDX measurements from Sample 1 are shown in Fig. 5, demonstrating that there is no evidence of Fe in the sample. The area in Figs. 5.(a-b) is approximately 50 microns across and mainly comprises Ca, O and Si. There are traces of Al, Sb, I and also Au/Pd. This particular sample was coated with Au/Pd in order to overcome issues with charging of the surface in the SEM. The EDX spectrum of the area shown in Fig 5. (c-d) is also dominated by Ca, O, Si and has no Fe.

For sample 2, mapping was carried out in the vicinity of the orange/brown area in Fig. 2(b). In Fig. 6(a), we show the appearance of the area in the SEM and the regions where EDX spectra were obtained on Sample 2. In Figs. 6(b) and (c), we show the EDX spectra for region 1 (on the orange area) and 2 (off the orange area), respectively. There is a significant difference in the composition of both areas - area 1 mostly comprises Fe, O, Si and Ca, whereas area 1 is mostly O, Si and Ca. The overall composition is much as expected: the sample consists of C, Si, O, Ca and various iron compounds. In Figs. 6(d-h), we show the elemental maps of Fe, Ca, Si, S and O, respectively from the area shown in Fig. 6(a). The orange/brown regions contain Fe which is either a form of pyrite (as evidenced by the presence of a small amount of S there) or an oxide. EDX on coccolith structures confirmed that they comprise almost exclusively of Carbon, Calcium and Oxygen. In Figs. 6(i-k), we show optical images of the same area.

We also conducted SEM/EDX on a Au/Pd coated (10 nm) section of sample 2, as shown in Fig. 7. With this more conductive coating, it is possible to obtain higher quality and more stable SEM images. We found this to be helpful when obtaining EDX spectra from this sample, as there tended to be excessive charging otherwise. In this area of sample 2, the sum spectrum shows Ca, O, Si, a small amount of Fe, and also some Na, K, Cl. This indicates this area has significant salt deposits, and verifies that it has not undergone washing. As was shown in Fig. 4(b), some areas are covered by a layer of material, and both it's appearance and the absence of any heavy metals or inorganic elements is consistent with reports of SEM on oil layers[9], as discussed above.

As well as characterizing the samples by optical and electron microscopy and EDX, an objective was to use AFM to explore the morphology of the surfaces in greater detail than either of these techniques allow.

AFM

AFM was used to explore the detailed topography of the coccoliths. The height information combined with high spatial resolution images complements the gross morphological and compositional information obtained by SEM. It became clear early on that the excessive roughness

associated with these samples would make repeated imaging in the same area extremely difficult, in all but a small number of regions. Fig. 8(a) shows an AFM image of a coccolith fragment from sample 1. Although it is not complete, the shape is consistent with a segment of an elliptical placolith of axial ratio approximately 2, where the short and long axes are 5 microns and 10 microns long, respectively. The thickness of the top of each of these overlapping plates is of order 60 nm, as shown in the cross-section in Fig. 8(b). Given that the inner rim edge appears to grow upwards from the shields, we believe that this particular coccolith fragment is upside-down and we are in fact observing the underside. In Fig. 8(c)-(d), we show other examples of coccoliths. In Fig. 8(c), the arrangement is similar to Fig. 8(a), in that the inner section of the rim is raised, indicating that we are again imaging the underside of a fragmented coccolith. In Fig. 8(d), the coccoliths are very small (overall diameter approximately 3 μm, with the central open area approximately 1 μm across), and are either muroliths or placoliths. Given the aspect ratio (the height is around 1 micron), these structures are most likely to be muroliths.

In Fig. 9, there are multiple coccolith fragments in close proximity to each other, all showing different characteristics. In the vast majority of heterococcoliths there is an outer part which is somewhat higher than the inner part of the coccolith. This provides a convenient basis for starting any description of the shape and structure of coccoliths. It also is in large part a reflection of the coccolithogenesis process; growth outward and upward from the proto-coccolith ring forms the outer rim whilst growth inward forms the central rim area [11]. The centre left of the image shows an asymmetric coccolith with a wing structure; the top centre shows a fragment of a placolith structure where the inner rim is lower than the outer one; resting on the left hand side of this last structure is a fragment of another coccolith on its side, this time consistent with the murolith shape.

Attempts at AFM imaging of sample 2 were hampered as a thin layer of material, presumed to be oil, covers many regions of the sample. This generally did not pose a problem in the SEM, as the more volatile components evaporated under the high vacuum conditions, and the paraffin-like components are reasonably stable, although as mentioned earlier, a thin coating of Au/Pd does make SEM imaging and EDX elemental mapping more straightforward. The AFM was carried out under ambient conditions, so there was continuous but slow evaporation of volatile compounds from the surface, some of which re-condensed on the AFM cantilever. This was manifested as a drift of the cantilever resonance frequency towards lower frequencies, rendering it a major challenge to obtain a stable tip-sample interaction during the course of an entire image, which was typically 15-20 minutes. In the regions where there was no layer, stable images were obtained showing a range of different types of material. In Fig. 10(a), some fragments of coccoliths are shown, and in Fig. 10(b), large cubic salt crystals are shown in an area that is apparently oil-free. These crystals have undergone partial dissolution, as can be seen by the rounded crystal apices and edges, and the appearance is consistent with that observed by SEM (Fig. 4(a). There were a number of cases where we were able to image what we believe to be the oily layer on the surface, as shown in Fig. 10 (Figs. 10(c), (e): topography, 10(d), (f): phase), which shows a 10 micron area. In Fig. 10(c) the layer is very smooth, and appears similar to what was observed in the SEM (Fig. 4(b)), and ascribed to the paraffin/waxy components of oil. The phase image of the same area, shown in Fig. 10(d) shows a difference in phase of over 40 degrees between the oil and the underlying surface, due to the fact that the oil is mechanically softer than the chalk. In a number of cases, we were also able to image a very thin layer of liquid that was weakly bound to the surface, as shown in Fig. 10(e). This is a 600 nm area, and the topography reveals small islands around 50-100 nm across. The thickness of this layer is of the order a few nm, and, while it is bound to the surface, it is laterally mobile. The phase image in Fig. 10(f) shows a drop in phase when the tip is above these islands, indicative of a stronger attractive

interaction between the probe and the layers than between the probe and the bare surface. The finding that the layer is non-uniformly distributed over the surface is in line with previous findings[2], [12] that showed the presence of localised hydrophobic patches on the surface.

The presence of Fe throughout sample 2, along with the related finding that there is a larger proportion of larger coccoliths (associated with Fe) led to the possibility that sample 2 might have interesting magnetic characteristics. The two samples, as well as a sample of crude oil from the same field were tested in a SQUID (superconducting quantum interference device) magnetometer.

SQUID

A small portion of each sample was placed in the SQUID magnetometer in turn, which applies a *H*-field and then measures the resulting magnetic moment (*M*) of the sample. The results are shown in Fig. 11. Sample 2 shows a largely paramagnetic response – there is no evidence of saturation up to the applied field of 60,000 Oe (6 Tesla). There is however a very small hysteresis (a slight difference between magnetisation on the backward and forward sweep), which is indicative of a small amount of weak ferromagnetism or ferrimagnetism. In contrast, sample 1 shows no magnetic response at all, nor does the crude oil sample that we investigated. To enable us to do so, the oil was cooled to 20K to make it solid.

Conclusion

Our measurements on two carbonate samples from the same position, but from different depths in the oil field in the North Sea reveal that the layer properties are highly inhomogeneous, and samples from these two depths have vastly different properties. Samples from higher up are yellow/grey in appearance and show coccoliths with less compaction and cementation, have less volatile organics and display no magnetic properties. The samples from the deeper layer contain coccoliths that are more compacted, evidence of clay, a layer of oil on the surface, and striking magnetic properties. It is almost certain that these differences are related. It is known that the addition of iron to plankton and algae promotes growth of these coccolithophores [7, 13], which leads to more coccoliths. It is therefore entirely consistent that sample 2 is (a) magnetic, (b) has more coccoliths that display overgrowth and cementation and (c) has more oil.

Acknowledgement

This work was carried out under the *NanoOil* project, funded by BP.

References

[1] R. Hoffmann, A. S. Wochnik, C. Heinzl, S. B. Betzler, S. Matich, E. Griesshaber, H. Schulz, M. Kučera, J. R. Young, C. Scheu, and W. W. Schmahl, "Nanoprobe crystallographic orientation studies of isolated shield elements of the coccolithophore species Emiliania huxleyi," *European Journal of Mineralogy*, vol. 26, no. 4, pp. 473-483, (2014).

[2] K. H. Enriksen, S. L. S. S. Tipp, J. R. Y. Oung, and M. E. M. Arsh, "Biological control on calcite crystallization : AFM investigation of coccolith polysaccharide function," *American Mineralogist*, vol. 89, no. 11–12, pp. 1709-1716, (2004).

[3] R. Hardman, "Chalk reservoirs of the North Sea," *Bulletin of the Geological Society of Denmark*, vol. 30, pp.119-137, (1982).

[4] M. D. Hollingsworth, "Chemistry. Calcite biocomposites up close," *Science*, vol. 326, no. 5957, pp. 1194-5, (2009).

[5] J. Brooks and B. Thusu, "Oil-source rock identification and characterization of the jurassic sediments in the northern north sea," *Chemical Geology*, vol. 20, no. 79, pp. 283-294, (1977).

[6] H. Lindgreen and F. Jakobsen, "Nano-quartz in North Sea Danian chalk," *Geological Survey of Denmark and Greenland Bulletin*, vol. 26, pp. 9-12, (2012).

[7] K. H. Coale, K. S. Johnson, S. E. Fitzwater, R. M. Gordon, S. Tanner, F. P. Chavez, L. Ferioli, C. Sakamoto, P. Rogers, F. Millero, P. Steinberg, P. Nightingale, D. Cooper, W. P. Cochlan, M. R. Landry, J. Constantinou, G. Rollwagen, A. Trasvina & R. Kudela, "A massive phytoplankton bloom induced by an ecosystem-scale iron fertilization experiment in the equatorial pacific ocean", *Nature*, vol. 383, pp. 495-501, (1996).

[8] R. van de Locht and T. Slater, "Ultrastructure and Crystallography of Nanoscale Calcite Building Blocks in Rhabdosphaera clavigera Coccolith Spines," *Crystal Growth & Design*, vol. 14, no. 4, pp. 1710–1718, (2014).

[9] R. G. Loucks, F. J. Lucia, and L. E. Waite, "Origin and Description of the Micropore Network within the Lower Cretaceous Stuart City Trend Tight-Gas Limestone Reservoir in Pawnee Field in South Texas," *GCAGS Joural*, vol. 2, no. 1, pp. 29-41, (2013).

[10] L. L. Skovbjerg, T. Hassenkam, E. Makovicky, C. P. Hem, M. Yang, N. Bovey & S. L. S. Stipp, "Nano-sized clay detected on chalk particle surfaces", *Geochimica et Cosmochimica Acta*, vol. 99, 57 (2012).

[11] K. H. Enriksen, S. L. S. S. Tipp, J. R. Y. Oung, and P. R. B. Own, "Tailoring calcite : Nanoscale AFM of coccolith biocrystals," *American Mineralogist*, vol. 88, no. 11–12, pp. 2040-2044, (2004).

[12] T. Hassenkam, a Johnsson, K. Bechgaard, and S. L. S. Stipp, "Tracking single coccolith dissolution with picogram resolution and implications for CO2 sequestration and ocean acidification.," *Proceedings of the National Academy of Sciences of the United States of America*, vol. 108, no. 21, pp. 8571-6, (2011).

[13] L. Stark, T. Emerson, C. Casipit, S. Brickey-Smith, and R. Douglas, "The Effects of Ocean Acidification on Meroplanktonic Organisms," *Alaska Oceans Sciences Bowl high school competition*, (2009).

Figure Captions

Fig. 1. Optical micrograph of sample 1 showing its complex morphology.

Fig. 2. Optical micrographs of sample 2: (a) overview and (b) a zoom-in on one of the orange/brown spots.

Fig. 3. SEM images of Sample 1. (a) and (b) show placolith structures, (c) shows a planolith structure and (d) shows a coccosphere. Surrounding these features, there are a large number of coccolith fragments. In both (c) and (d), the scale bar is 1 μm. The inner and outer rims referred to in the text are indicated in Fig. 3(b) as *IR* and *OR*, respectively.

Fig. 4. SEM of sample 2. (a) In this area, several coccolith fragments (C) can be seen, as well as salt crystals; (b) a nearby area with a coccolith fragment mostly covered in oil; (c) coccolith surface showing dendritic clay deposits. In each case, the scale bar is 1 μm.

Fig. 5. Sample 2 (a) SEM image of the area where EDX spectra were obtained. The orange/brown area is indicated by the white dashed outline. Area 1 was on top of this structure, and area 2 was around 10 microns away. (b) EDX sum spectrum averaged over area 1 (red line) and area 2 (black line); (c)-(g) elemental maps of Fe, Ca, Si, S and O, respectively. (h)-(j) Optical images of this area.

Fig. 6. Au/Pd Coated Sample 1 (a) SEM image of an area centred on a planolith where EDX spectra were obtained. (b) EDX sum spectrum averaged over this area.

Fig. 7. Au/Pd Coated Sample 2 (a) SEM image of the area where EDX spectra were obtained (b) EDX sum spectrum averaged over this area- Al peak is indicative of clay, consistent with the dendrites observed on the coccolith surface shown in Fig. 4(c); (c)-(g) elemental maps of Ca, Si, Cl, Na and O, respectively.

Fig. 8. AFM images of coccolith fragments (a) a section of an elliptical coccolith, (b) cross-section along line shown in (a) showing that the step height between the platelets is of order 60 nm; (c) and (d) coccolith fragments.

Fig. 9. AFM image of coccolith fragments showing several different morphologies, including an asymmetric ellipse (*E*), a placolith (*P*) and a murolith (*M*).

Fig.10. AFM images of plug B showing (a) coccoliths; (b) Salt crystals (image size 10 microns); (c)-(f) Oily film on the surface; (c) and (e) are topography whereas (d) and (f) are the corresponding phase images. The scale bars in (b)-(d) are 1 micron, and those in (e)-(f) are 100 nm.

Fig. 11. SQUID measurement on samples 1 & 2 & crude oil.

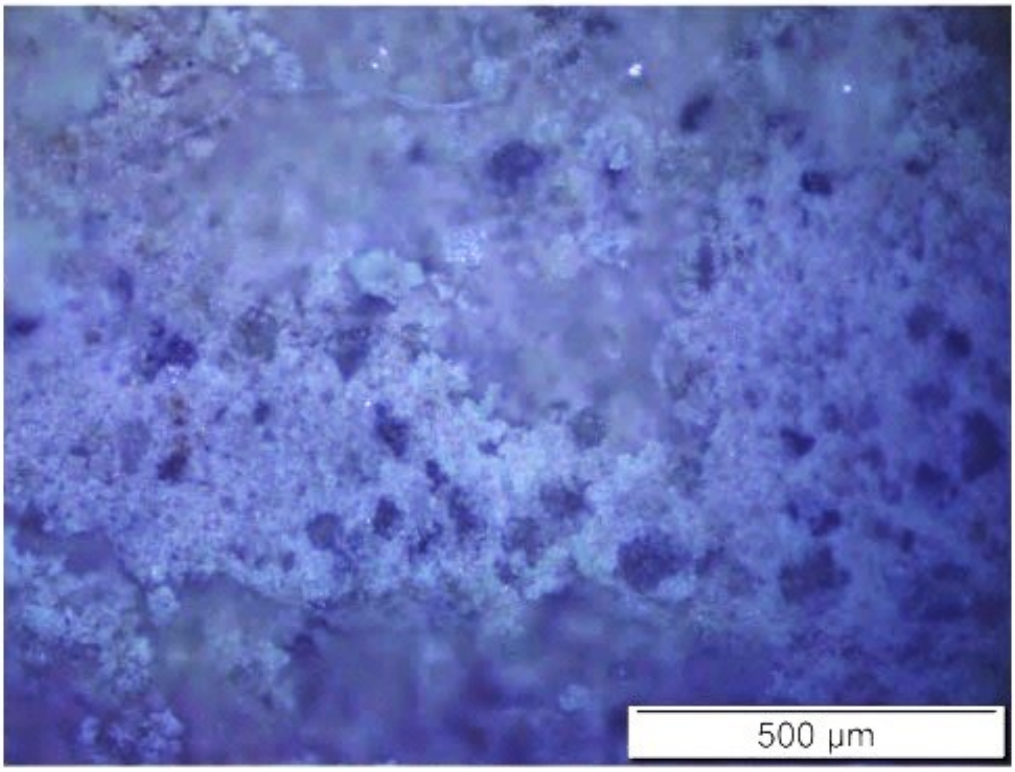

Fig. 1 Optical micrograph of sample 1 showing the complex morphology.

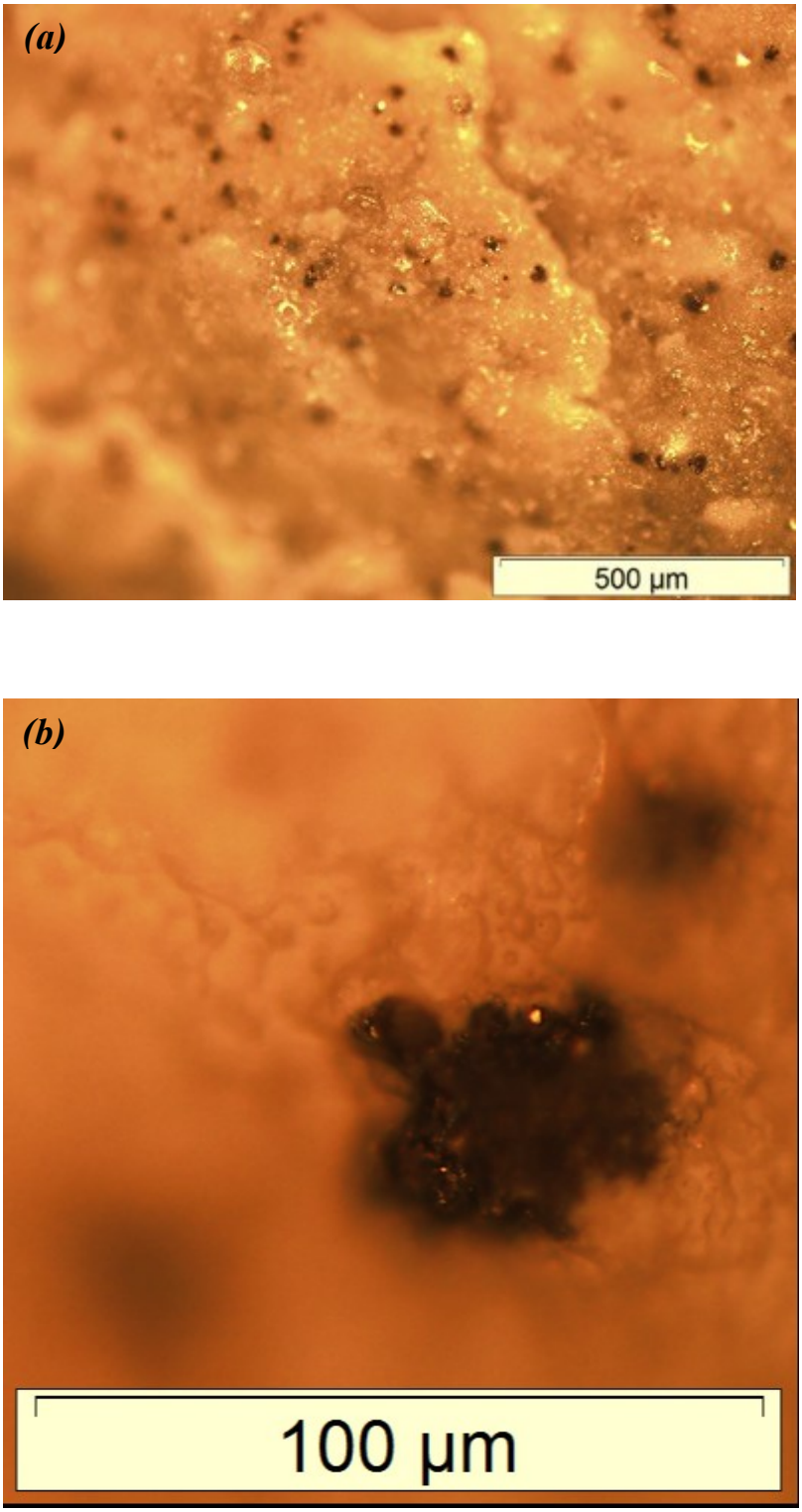

Fig. 2 Optical micrographs of sample 2: (a) overview and (b) a zoom-in on one of the orange/brown spots.

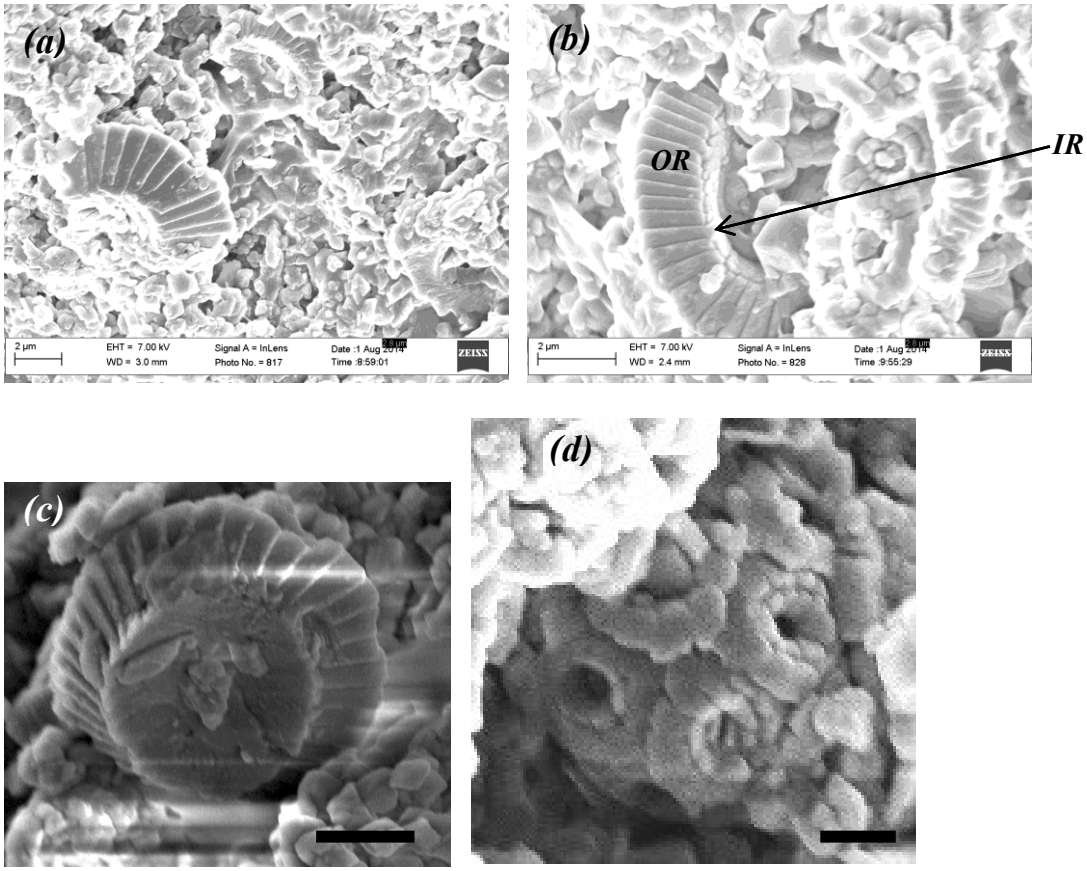

Fig. 3 SEM images of Sample 1. (a) and (b) show placolith structures, (c) shows a planolith structure and (d) shows a coccosphere. Surrounding these features, there are a large number of coccolith fragments. In both (c) and (d), the scale bar is 1 μm. The inner and outer rims referred to in the text are indicated in Fig. 3(b) as *IR* and *OR*, respectively.

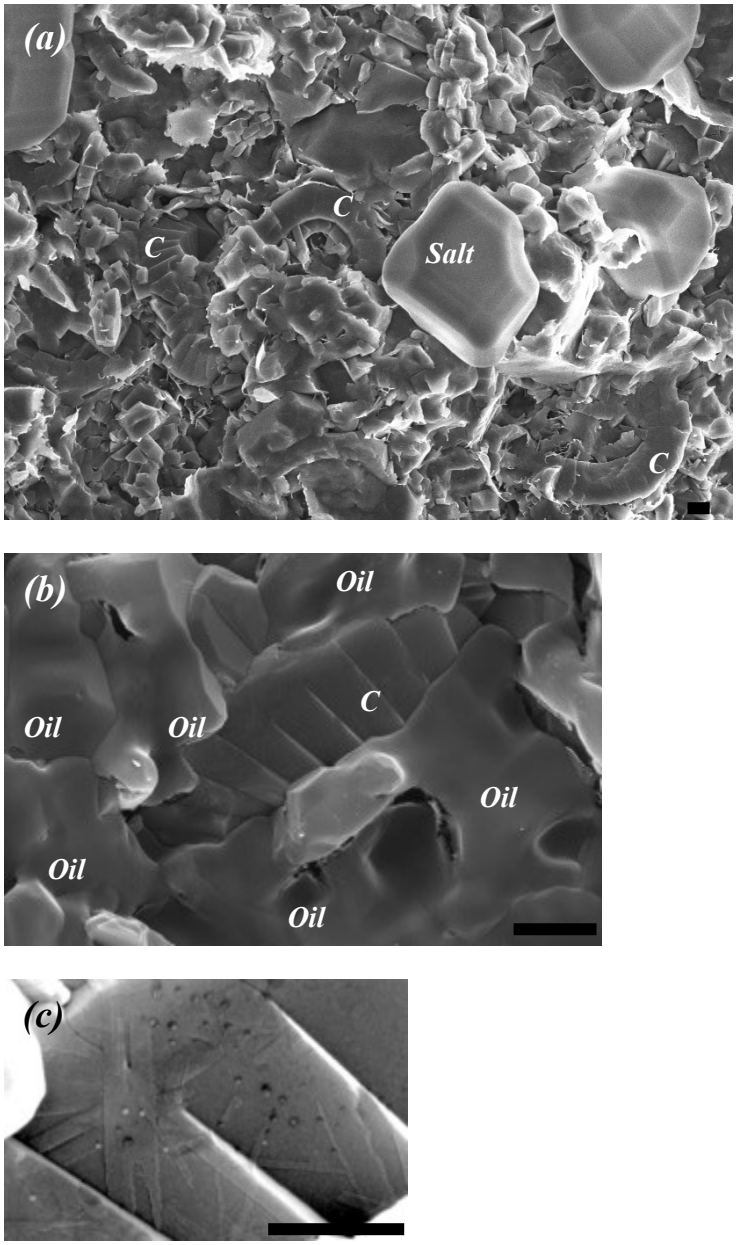

Fig. 4 SEM of sample 2. (a) In this area, several coccolith fragments (C) can be seen, as well as salt crystals; (b) a nearby area with a coccolith fragment mostly covered in oil; (c) coccolith surface showing dendritic clay deposits. In each case, the scale bar is 1 μm.

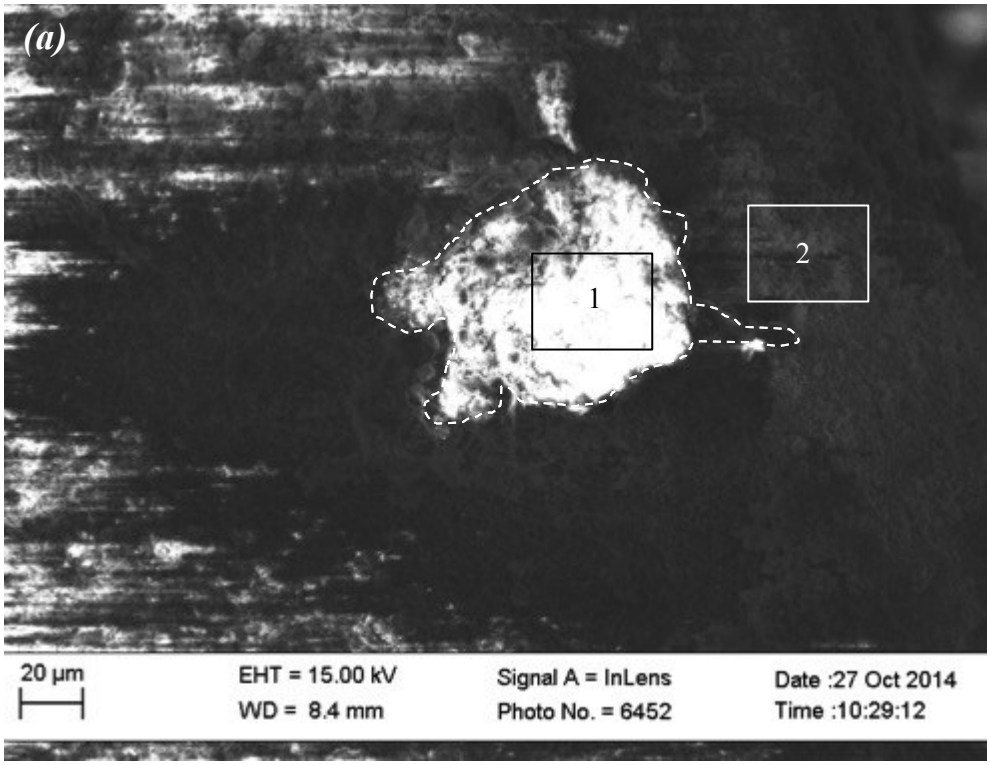
(a)
1
2
20 µm
EHT = 15.00 kV
WD = 8.4 mm
Signal A = InLens
Photo No. = 6452
Date :27 Oct 2014
Time :10:29:12

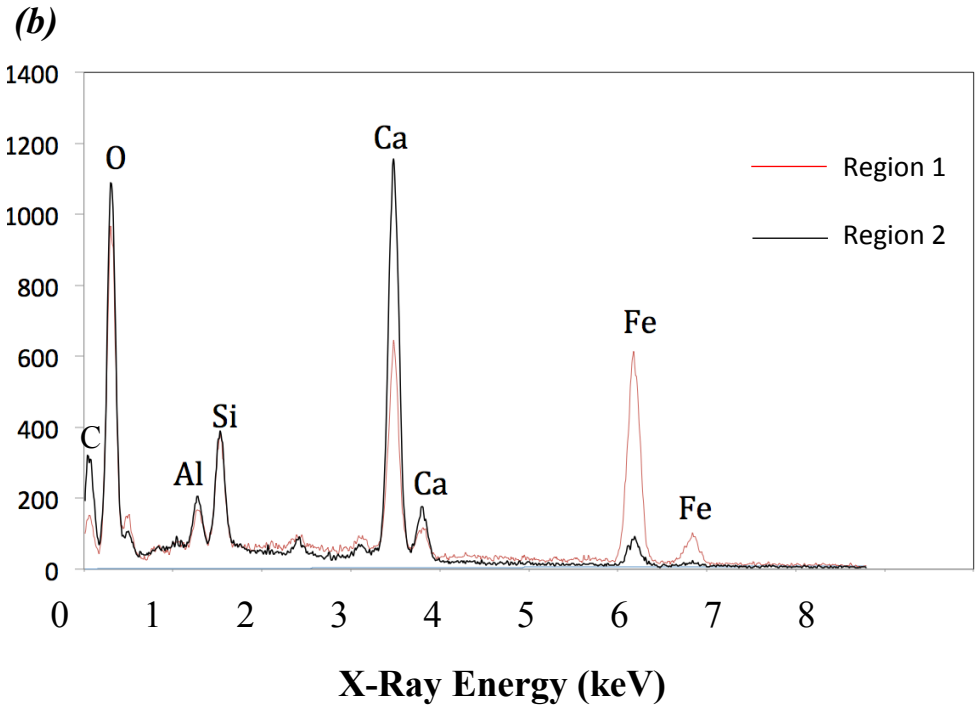
(b)
1400
1200
1000
800
600
400
200
0
0
1
2
3
4
5
6
7
8
O
Ca
Si
C
Al
Ca
Fe
Fe
Region 1
Region 2
X-Ray Energy (keV)

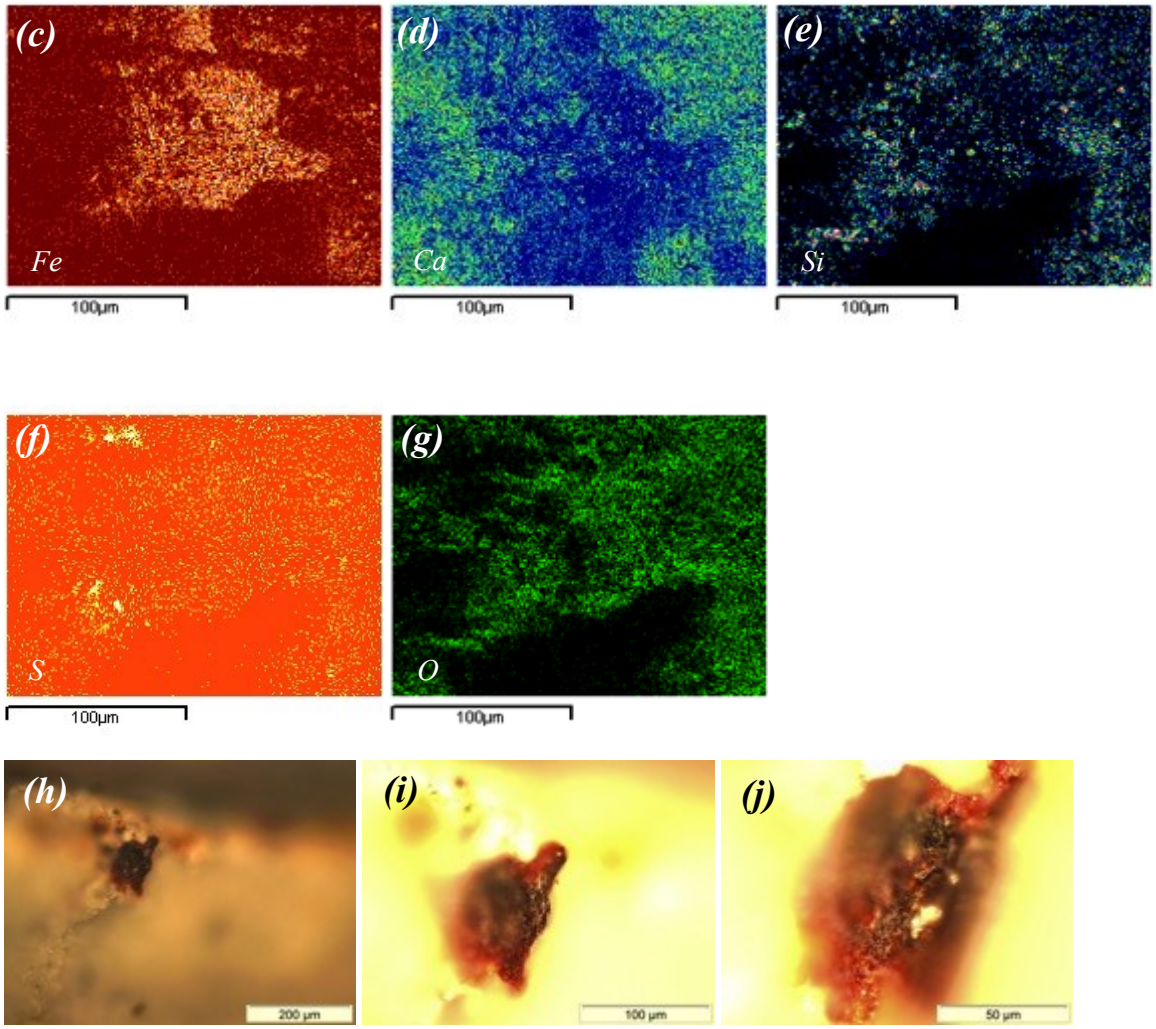

Fig. 5. Sample 2 (a) SEM image of the area where EDX spectra were obtained. The orange/brown area is indicated by the white dashed outline. Area 1 was on top of this structure, and area 2 was around 10 microns away. (b) EDX sum spectrum averaged over area 1 (red line) and area 2 (black line); (c)-(g) elemental maps of Fe, Ca, Si, S and O, respectively. (h)-(j) Optical images of this area.

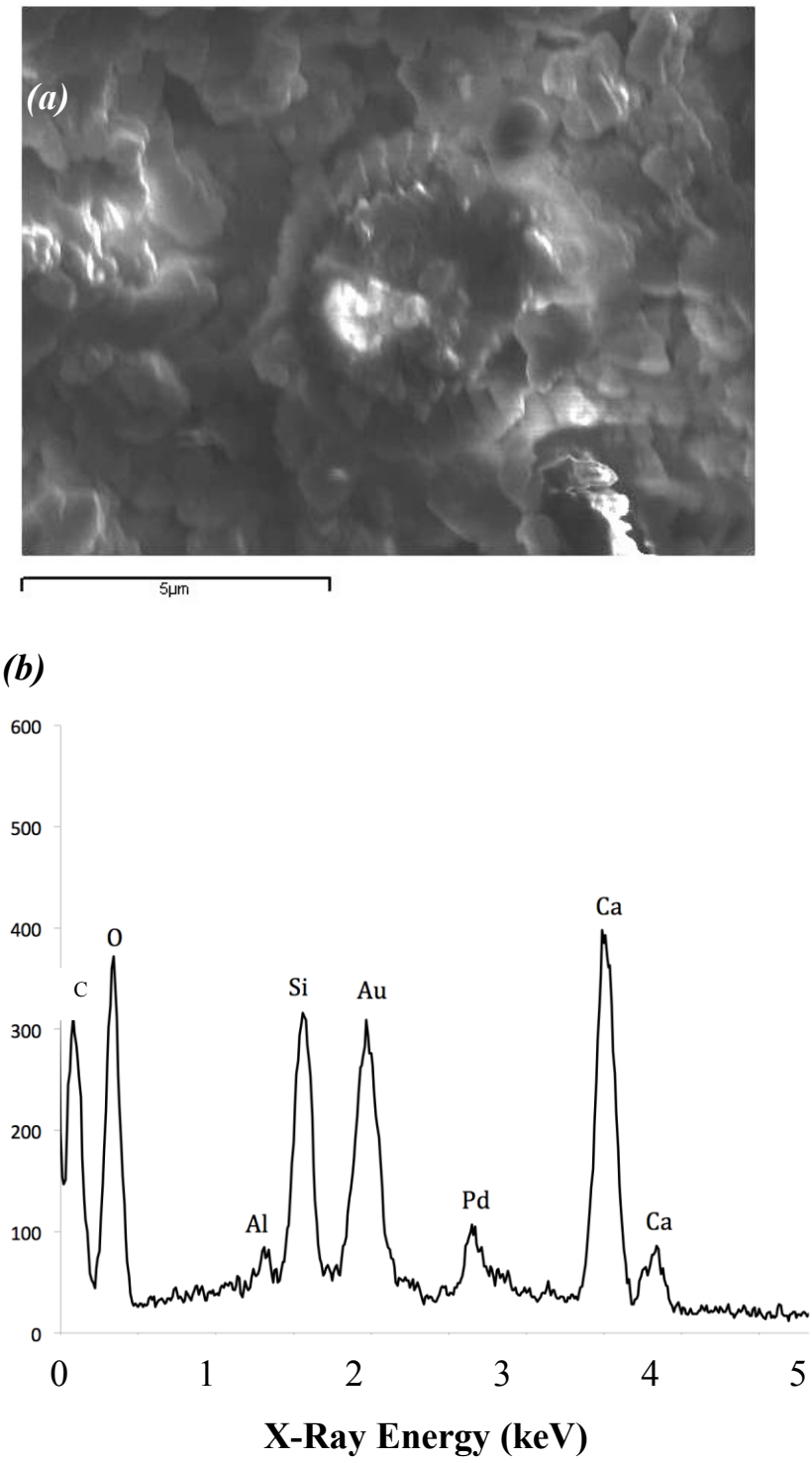

Fig. 6. Au/Pd Coated Sample 1 (a) SEM image of an area centred on a planolith where EDX spectra were obtained. (b) EDX sum spectrum averaged over this area.

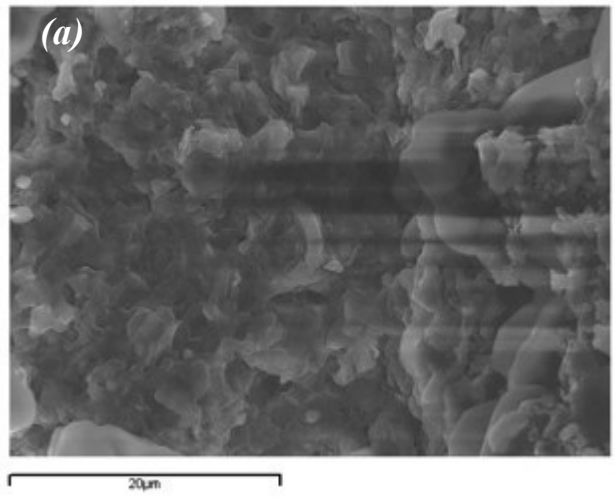
(a)
20µm

(b)

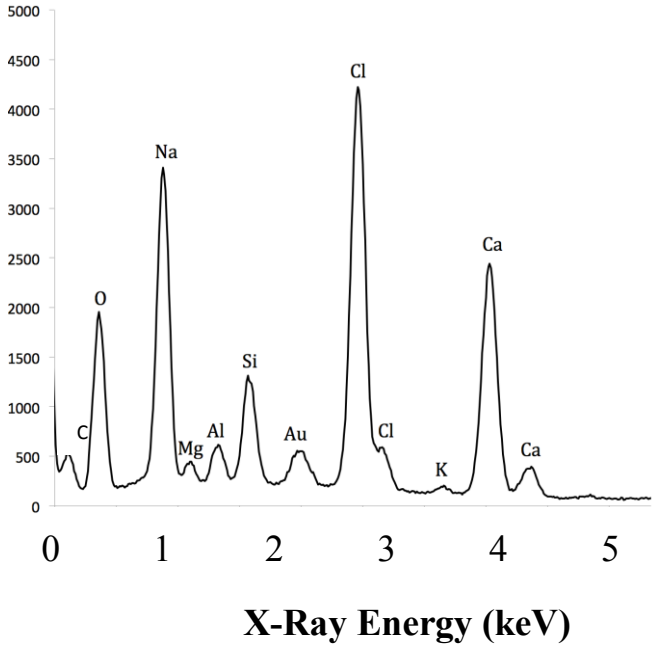
5000
4500
4000
3500
3000
2500
2000
1500
1000
500
0
C
O
Na
Mg
Al
Si
Au
Cl
Cl
K
Ca
Ca
0
1
2
3
4
5
X-Ray Energy (keV)

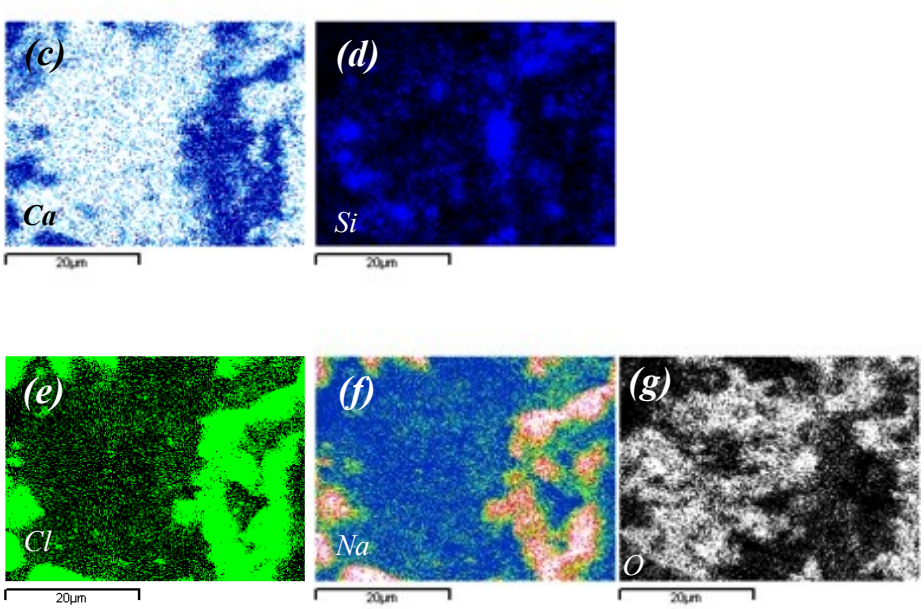

Fig. 7. Au/Pd Coated Sample 2 (a) SEM image of the area where EDX spectra were obtained (b) EDX sum spectrum averaged over this area- Al peak is indicative of clay, consistent with the dendrites observed on the coccolith surface shown in Fig. 4(c); (c)-(g) elemental maps of Ca, Si, Cl, Na and O, respectively.

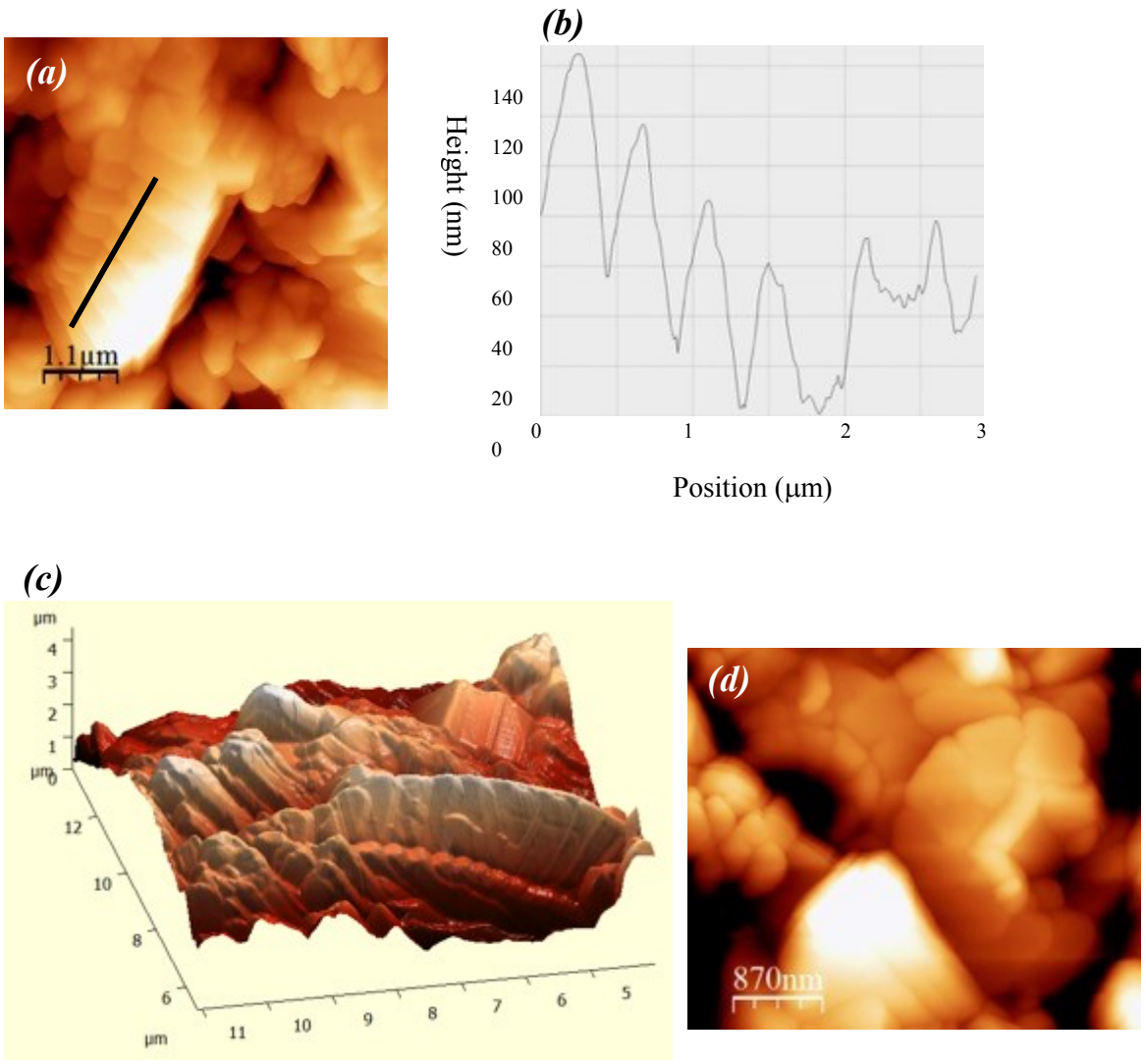

Fig. 8. AFM images of coccolith fragments (a) a section of an elliptical coccolith, (b) cross-section along line shown in (a) showing that the step height between the platelets is of order 60 nm; (c) and (d) other coccolith fragments we observed with different shapes.

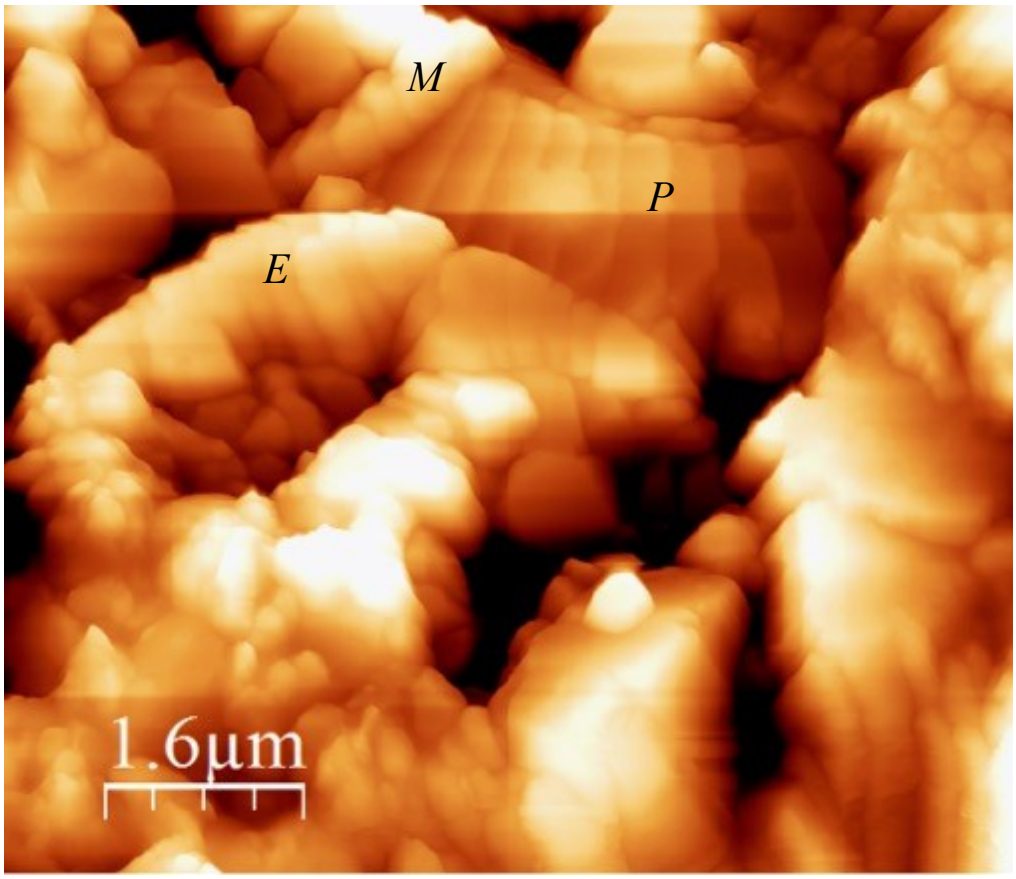

Fig. 9. AFM image of coccolith fragments showing several different morphologies, including an asymmetric ellipse (*E*), a placolith (*P*) and a murolith (*M*).

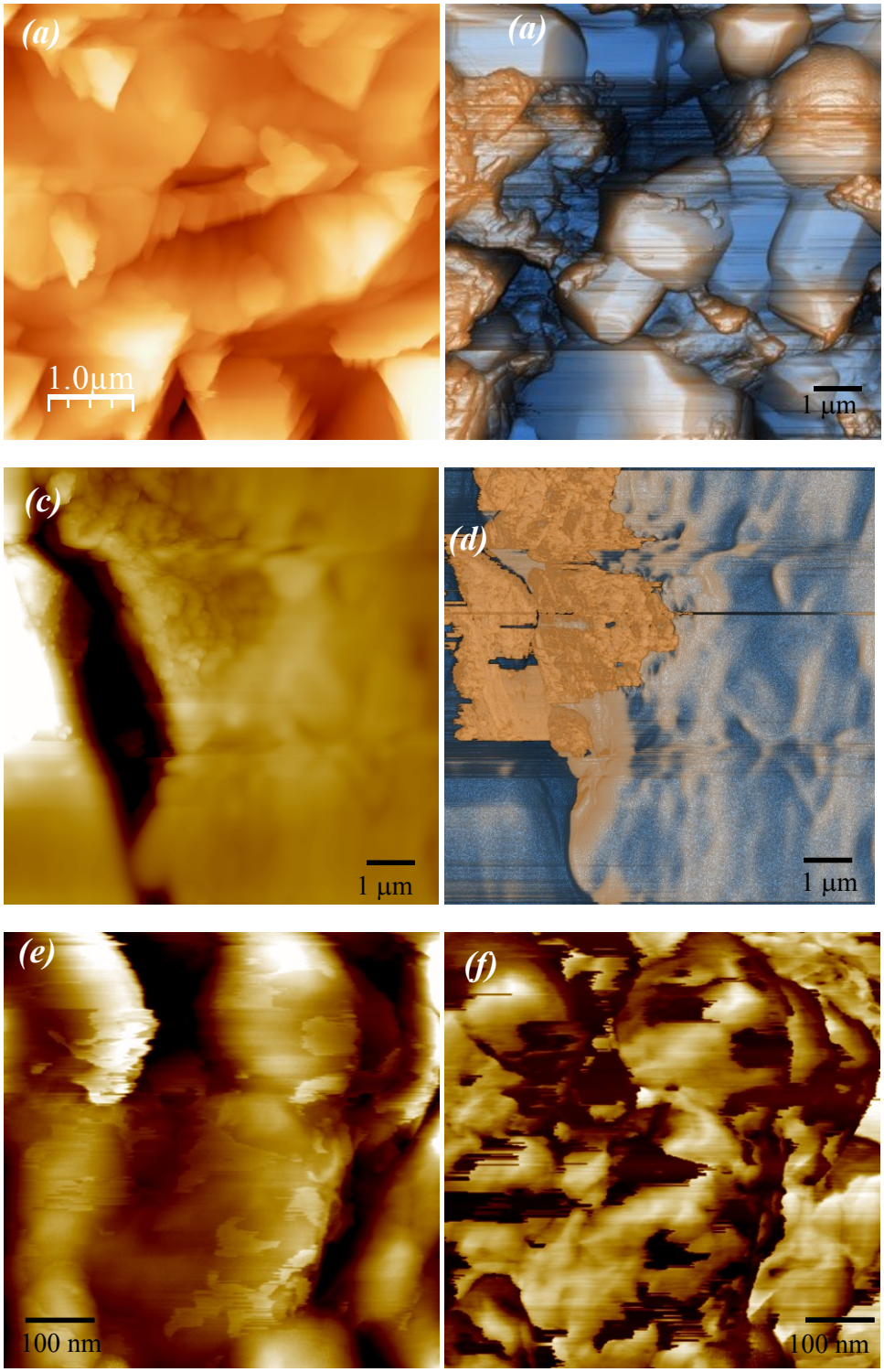

Fig.10. AFM images of plug B showing (a) coccoliths; (b) Salt crystals (image size 10 microns); (c)-(f) Oily film on the surface; (c) and (e) are topography whereas (d) and (f) are the corresponding phase images. The scale bars in (b)-(d) are 1 micron, and those in (e)-(f) are 100 nm.

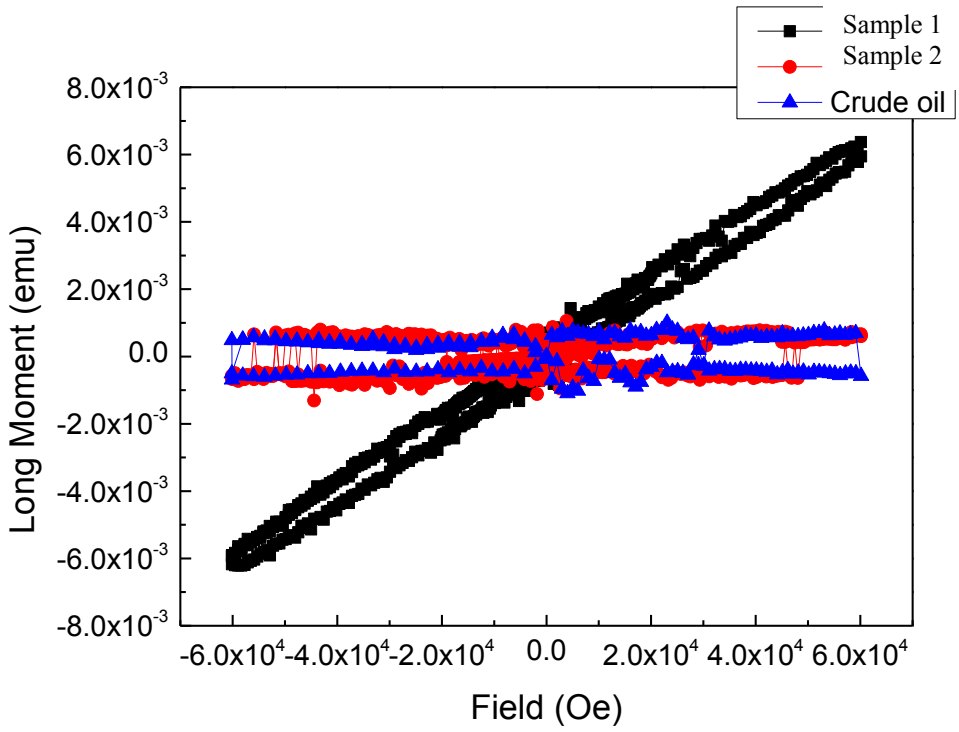

Fig. 11. SQUID measurement on samples 1 & 2 & crude oil.